The Characterization of Scanning Noise and Quantization on Texture Feature Analysis

G. Martin[1], M.S. Pattichis[1,2]

[1]*image and video Processing and Communications Lab (ivPCL)*
Department of Electrical and Computer Engineering
The University of New Mexico, Albuquerque, NM 87131-1356
[2]*Department of Computer Science*
The University of Cyprus, CY-1678, Cyprus
gdmart@sandia.gov, pattichis@ece.unm.edu

Abstract

The study of the effects of scanning on texture features is of great interest to computer-based screening systems. A mathematical model is developed for understanding how the original image gets distorted due to contrast variability and geometric distortion inherent in the scanning process. Both quantitative and qualitative results (for sixty common texture features) are given.

1. Introduction

With the current integration of digital technology in medicine and the development of digital diagnostic tools (i.e. Automated Screening Systems); there has become an increasing need to digitize analog radiograph images. This process is accomplished through the use of laser scanners or charge-coupled device (CCD) scanners. Despite routine calibration and quality control, both types of scanners have operational constraints which introduce various artifacts.

A quantitative approach as suggested by Halpern [1] uses a calibrated test pattern for direct quality control with the digital media. This test pattern is designed to help characterize the various scanning artifacts and noise. An example test pattern is shown in Figure 1. In our paper, we will use the test pattern in Figure 1 to describe many of the artifacts associated with the scanning process.

A mathematical model for describing the distortion of the original image due to the scanning process will also be developed. Our model will focus on the contrast and geometric distortions. We will not discuss sampling and quantization issues.

The rest of the paper is organized into five Sections: the methods, the mathematical model for scanning Section, the texture feature section, the results, and the conclusion.

2. Methods

2.1 Apparatus

The digitization device is a Vidar VXR-12 CCD Scanner with optical density range of .00 – 3.85 in optical density units. The VXR-12 is equipped with a 16-bit depth sensor array for scanning. The scanner also has many features, which can be controlled through the TWAIN32 software package. Some of these features include line averaging, dark enhance,
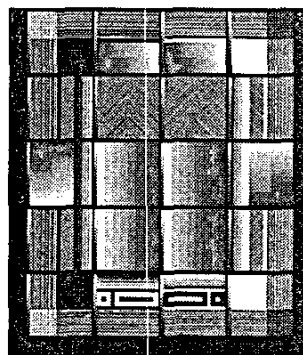

Figure 1. The Film Test Pattern. The test pattern consists of 20 squares, numbered from left to right, top to bottom.

exposure time (10 – 40ms), and various look-up tables.

152

The scanner is also able to scan at multiple resolution levels (72 – 570 dpi). For the experiments conducted, the scanner was set at 300 dpi with a 12-bit pixel depth and a linear look up table. The exposure time was set to an optimized value based on contrast and entropy.

The calibrated film test pattern (Figure 1) is based upon a widely used test pattern from The Society of Motion Picture and Television Engineers (SMPTE). It is however, specifically designed to evaluate laser and CCD digitizers. The film itself is calibrated so that it varies less than .10 optical density units from the digital synthetic pattern. This is easily verified with a densitometer.

2.2 Procedure

Digitizer performance was tested both subjectively and quantitatively. The various subjective and quantitative test measures performed are described with their associated squares on the film test pattern as follows:

• *High Contrast Discrimination* – Determined by the horizontal, vertical and diagonal line pairs. The limiting resolution is defined in terms of the distance where the excursion of the profile is one third of its original amplitude. This is associated with squares numbered 1-8 and 13-20, testing vertical and horizontal (1,4,17,20), horizontal only (2,3,18,19), vertical only (5,8,13,16), and diagonal (6,7) contrast discrimination.

• *Low Contrast Discrimination* – Determined by the number of low contrast squares visible in each column of the center step gradients. The squares are ~9% different in optical density units from the gradient bar containing them. The limiting contrast is defined as the square where the pixel values are one third of the values in the largest square. This is associated with squares numbered 10, 11, 14, 15.

• *Gray Scale Response* – Determined by each of the 16 steps in the step gradients, which should be visibly distinct from the adjacent steps. The mean pixel value at each step can be plotted against the known optical density units to determine the gamma correction factor for the scanner. The standard deviation of pixels in each step, when plotted against the known optical density units, can be used to measure the relationship of noise to optical density. There are gradient bars located next to each of the 20 segments in the test pattern. These will help determine whether there is spatial variation in gray-scale response across the image. Every square has a vertical step gradient bar on the left. The squares numbered 9 and 12 have large step vertical gradient bars/linear gradients, while 2 and

3 have large horizontal step gradient bars/linear gradients.

• *Fine Line Reproduction* – Determined by the fine lines within the test pattern, which should be visible and continuous. This is associated with squares numbered: 5, 8, 9, 12, 13, 16, 18, and 19. The squares numbered 5, 8, 9, 12, 13, 16 have vertical fine lines within gradients, while 18 and 19 have horizontal fine lines in gradients.

• *Geometric Distortion* – Determined by the 20 square segments of the test pattern. Each segment is the same size and square except for the added step gradient bar to the left of each segment. Squares numbered 18 and 19 have special patterns to check geometric distortion.

• *Homogeneity* – Quantization noise will be evident in the regions that exhibit constant gray level properties. Random independent noise can also be observed within the constant gray level regions of the test pattern. A plot of standard deviation of the pixel values versus the known optical density units for the area under observation will help relate optical density to noise. For testing homogeneity, we can use the first border of the entire image, and squares numbered 1,4,17, and 20 which have constant regions.

• *Film Movement* – Determined by the line pairs, which should appear straight, and there should not be any stretching or splicing along the horizontal and vertical axes. This is associated with squares numbered 1, 4, 5, 8, 13, 16, 17, and 20. We can use vertical line pairs for horizontal movement and horizontal line pairs for vertical movement. We can also examine the entire test pattern image for possible rotations.

• *Light Leakage* – Determined by the black border around the image and separating each of the 20 square segments. These border areas should not contain any light areas which may have leaked from an external source, or the adjacent segments. This can be checked by examining the borders of the scanned image, and all squares with line pairs, such as the squares numbered 18 and 19.

3. A Model for Scanning Distortions

In this Section, we develop a mathematical model for describing different artifacts due to the scanning process. We primarily focus on geometric distortions and contrast variation. To help recognize the effects on different statistical features, we first develop a spatial model and then derive its effects on the spectral model.

Let the original image be denoted by $h(x_1, x_2)$. We want to model contrast variation residual effects after any sensor corrections, such as gamma correction, have been applied. We use a positive amplitude

function $a(x_1,x_2)$ to account for the variability, and write $a(x_1,x_2)h(x_1,x_2)$ for the contrast-altered image.

We note that image contrast can be enhanced through processing the scanned image. Also, we note that although image contrast is extremely important for visual screening, its impact on computer-based screening is not so clear.

We model *geometric distortion* and *film movement* as a coordinate transformation

$$\Phi\,(x_1,x_2)=(\phi_1\,(x_1,x_2),\,\phi_2\,(x_1,x_2))$$

where the original image coordinate points (x_1,x_2) get mapped to $(\phi_1\,(x_1,x_2),\,\phi_2\,(x_1,x_2))$. Without loss of generality, we write the more general expression

$$g(x_1,x_2)=a\,(x_1,x_2)\,h\,(\phi_1(x_1,x_2),\,\phi_2(x_1,x_2)) \quad (1)$$

expressing the scanned image $g(x_1,x_2)$ in terms of the original, continuous-space image $h(x_1,x_2)$.

The *fine line reproduction* characteristic suggests the introduction of a band-limited assumption for the scanned image. To relate the band-limited assumption to the original image, we begin with the two-dimensional Fourier Transform expression for h given by

$$h(x_1,x_2)=\iint H(f_1,f_2)\exp[j2\pi(f_1x_1+f_2x_2)]df_1df_2\,.$$

From (1), we have that the scanned image can be expressed in terms of the Fourier Transform expansion of the original image using

$$g(x_1,x_2)=\iint H(f_1,f_2)\,a(x_1,x_2)\exp[j2\pi(f_1\phi_1(x_1,x_2)$$
$$+\,f_2\phi_2(x_1,x_2))]\,df_1df_2 \quad (2)$$

From (2), we see that if the original signal is band-limited within the x_1-x_2 coordinate system, the scanned image will also be band-limited for the same frequency region within the deformed $\phi_1-\phi_2$ coordinate system. Alternatively, it is easy to see that if we assume that the scanned image is band-limited within the x_1-x_2 coordinate system, the original image will have to be band-limited for the inverse-coordinate system Φ^{-1}. Thus, it is clear that a band-limited assumption for a particular coordinate system can lead to band-limitness for another coordinate system through a change of variables. For simplicity, we assume that the scanned image is band-limited with respect to the deformed $\phi_1-\phi_2$ coordinate system. In addition, we simplify our expressions for real images.

Let $H(f_1,f_2)=|H(f_1,f_2)|\exp[j\theta(f_1,f_2)]$ be the polar representation of the Fourier Transform of the original image. Due to the conjugate symmetry in the Fourier Transform of real images, we only consider the

right half of the spectrum of the scanned image, introduce the factor of 2 as a correcting factor, to get

$$g(x_1,x_2)=2\iint H(f_1,f_2)a(x_1,x_2)$$
$$\cos\Phi(x_1,x_2,f_1,f_2)df_1df_2$$

where

$$\Phi(x_1,x_2,f_1,f_2)=f_1\phi_1(x_1,x_2)+f_2\phi_2(x_1,x_2)$$
$$+\,\theta(f_1,f_2).$$

The scanned image can be approximated by

$$g(x_1,x_2)\cong 2Ma(x,x)\cos\Phi(x_1,x_2,f_{1,m},f_{2,m}) \quad (3)$$

where:

$$M=\iint H(f_1,f_2)df_1df_2\,,$$

$$f_{1,m}=\frac{1}{M}\iint f_1|H(f_1,f_2)|df_1df_2$$

$$f_{2,m}=\frac{1}{M}\iint f_2|H(f_1,f_2)|df_1df_2$$

The film test patterns are usually restricted to be made up of lines of pixels. This motivates our model for the Fourier spectrum of the original image as a line-spectrum, along (say) the f_1-direction: $H(f_1,f_2)=H(f_1)\delta(f_2)$. We can show, (through a long derivation), that in this case, the error is bounded above by (omitted due to lack of space):

$$|g(x_1,x_2)-2M\,a\,(x_1,x_2)\cos\Phi(x_1,x_2,f_1,f_2)|$$
$$\leq a\,(x_1,x_2)\,P_{2,0}\left(\Phi^2_{f_1,\sup}(x_1,x_2)+\theta_{f_1,f_1,\sup}\right)$$

where:

$$h_1=f_1-f_{1,m}$$
$$h_2=f_2-f_{2,m}$$

$$P_{n,m}=\iint|h_1|^n|h_2|^m|H(f_1,f_2)|df_1df_2,\quad n,m=1,2,3,\ldots$$

$$\theta_{f_1,f_1,\sup}=\sup_{(f_1,f_2)}\left|\frac{\partial^2\theta}{\partial f_1^2}(f_1,f_2)\right|$$

$$\Phi_{f_1,\sup}(x_1,x_2)=\sup_{(f_1,f_2)}\left|\frac{\partial\Phi}{\partial f_1}(x_1,x_2,f_1,f_2)\right|$$

We return to (3) to note that our model can be used to predict the distortion to both the phase and the amplitude of each Fourier Harmonic of the original image. Furthermore, it is clear that the distortion is also a function of the spread of the spectrum of the original image. In general though, we can see that significant changes to the phase can occur as a result of geometric distortions.

4. Statistical Texture Feature Analysis

For the statistical feature analysis, we used 60 common texture features that are often used in screening systems. These features are sorted into sets as follows:

- First Order Statistics
  Mean, Median, Mode, Variance, Skewness, Kurtosis, Energy, Entropy.
- Spatial Gray Level Dependence Matrices [3]
  Angular Second Moment, Contrast, Correlation, Sum of Squares: Variance, Inverse Difference Moment, Sum Average, Sum Variance, Sum Entropy, Entropy, Difference Variance, Difference Entropy, and two Information Measures of Correlation. There are four angular gray level dependence matrices for each of the above 13 texture measures. The mean and the range of the four values of each of the 13 texture measures comprise a set of 26 texture features.
- Gray Level Difference Statistics
  Contrast, Angular Second Moment, Entropy, Mean
- Neighborhood Gray Tone Difference Matrix [2]
  Coarseness, Contrast, Busyness, Complexity, Strength.
- Statistical Feature Matrix
  Coarseness, Contrast, Periodicity, Roughness
- Laws Texture Energy Measures [5]
  LL, EE, SS, LE, ES, and LS Kernel Energies
- Fractal Dimension Texture Analysis [4, 6]
  Hurst Coefficients (4 resolutions)
- Fourier Power Spectrum [7]
  Radial Sum, Angular Sum.

The 60 features in each of the 8 sets are calculated for all 20 of the segmented squares in the synthetic test pattern and for 50 scan trials of the segmented squares in the digitized film pattern. The sample size of 50 was chosen, because it is where the mean of each individual feature started to converge to a specific value. The convergent value mean is compared to the feature value for the synthetic digital image with both the T-Test and Wilcoxon Rank Sum Test. Statistical significance and feature sensitivity to scanning noise is determined at an $\alpha = .05$.

5. Results

5.1 Qualitative Results

In this subsection, different experiments are described that are used to demonstrate different visual artifacts.

The *high-contrast resolution* experiments exhibited a large amount of sampling noise. These errors can be attributed to the limitations on the film feeder within the scanner and the resolution of 300 dpi.
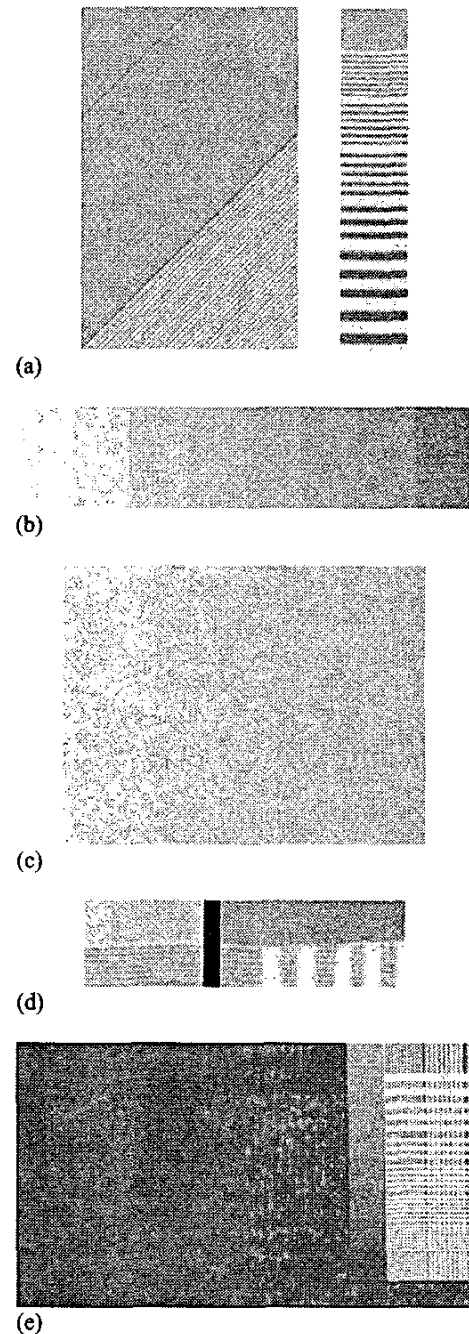

(a)

(b)

(c)

(d)

(e)

Figure 2. Artifacts in the scanned images.

The motion of the film through the feeder brought about aliasing effects that were noticeable in all three

directions of the High contrast line pairs. We note the blurring effect with the higher resolution line pairs in Figure 2(a).

The *low-contrast discrimination* experiments exhibited some quantization noise within the higher intensity portion of the step gradient. In Figure 2(b), we note that the small, low contrast blocks were in some cases not visible.

The *gray-scale response* gradients show a slightly logarithmic nature compared to the linear nature of the synthetic digital image. This effect was expected due to the gamma parameter of the scanner. The unexpected problems with the gray scale response were the random noise and quantization artifacts seen in the continuous gradient function. In Figure 2(c), we note that the edges between levels are jagged from quantization and this creates a "sand dune" or "water ripple" effect.

The *fine line reproduction* has the aliasing effects discussed earlier, which cause the highest resolution line pairs (3.5 lp/mm) to appear as a constant block. The *geometric distortion* was negligible and both images retained the same distance measure for each side of the segmented squares. *Film movement* was noticeable for each of the scanning trials. In Figure 2(d), we note the split in the vertical line pairs that appear as a warped line. Also, we note the complete horizontal shift present less than 500 pixels below the warping.

Light leakage is noticeable in the borders of the scanned images. This can be seen as light shadows. In Figure 2(e), we note the striping effect from the lines that will be scanned.

3.1 Quantitative Results

Overall, even with Gamma correction, the statistical tests showed a significant difference between the optical density in the original image and the scanned copies. The difference was significant enough to affect all the features. This difference will most likely be significantly less for laser scanners.

Nevertheless, we are still extremely interested in the variability of the scanned copies. Significant variability is a sign of instability in a texture feature, and it should be taken into account when using the features for computerized screening.

We note that most of the variability was not large. For example, for the mean of the pixels in each square, we found that the maximum of the mean absolute difference was about 0.5, when the mean value varied from 100 to 200. Thus the difference is less than 0.25%.

Resolution problems such as in fine line reproduction can have a significant effect on the variance of the features. For example, for square numbered 19, fifteen out of the sixty features exhibited their largest variance over all the other squares. Both spectral-domain features exhibited their largest variance over square numbered 19. This observation motivates the further study of the spectral domain variability due to scanning (see Section 3).

Scanning artifacts affecting high contrast discrimination and homogeneity can also have a significant effect on the variance of the features. For example, for squared number 4, fourteen out of the sixty features exhibited their largest variance over all the other squares.

In general though, we cannot really associate single squares with specific scanning artifacts (see Section 2). This observation further complicates the analysis.

6. Conclusions

Scanning artifacts do increase the variance of textural features used for computer screening. The use of mathematical scanning models can help us understand the extends of the effects of the artifacts.

7. References

[1] E. Halpern, "A Test Pattern for Quality Control of Laser Scanner and Charge-Coupled Device Film Digitizers", *Journal of Digital Imaging*, Vol. 8, No 1, Feb. 1995: pp 3-9

[2] M. Amadasun, R. King, "Textural Features Corresponding to Textural Properties", *IEEE Transactions on Systems, Man, and Cybernetics*, Vol. 19, No 5, Sept/Oct 1989, pp 1264-1274

[3] R.M. Haralick, K. Shanmugam, I. Dinstein, "Texture Features for Image Classification", *IEEE Transactions on Systems, Man., and Cybernetics*, Vol. SMC-3, Nov 1973, pp. 610-621

[4] H. Lauwerier, *Fractals, Endlessly Repeated Geometrical Figures*, Princeton University Press, Princeton, New Jersey.

[5] K.I. Laws, "Rapid Texture Identification", *SPIE*, 1980, Vol. 238, pp. 376-380.

[6] B.B. Mandelbrot, *The Fractal Geometry of Nature*, San Francisco, CA, Freeman.

[7] J.S. Weszka, C.R. Dyer, A. Rosenfield, "A Comparative Study of Texture Measures for Terrain Classification", *IEEE Transactions on Systems, Man. & Cybernetics*, Vol. SMC-6, 1976, pp. 269-285

[8] Wu Chung-Ming, Chen Yung-Chang, "Statistical Feature Matrix for Texture Analysis", *CVGIP: Graphical Models and Image Processing*, Vol. 54, No 5, Sept 1992, pp 407-419.

[9] Wu Chung-Ming, Chen Yung-Chang, Hsieh Kai-Sheng, "Texture Features for Classification of Ultrasonic Liver Images", *IEEE Transactions on Medical Imaging*, Vol. 11, No 2, 1992, pp 141-152.